HHS Public Access

Author manuscript

Med Phys. Author manuscript; available in PMC 2024 November 01.

Published in final edited form as:

Med Phys. 2023 November ; 50(11): 6836–6843. doi:10.1002/mp.16712.

Technical Note: Exploring the Detectability of Coronary Calcification using Ultra-high-resolution Photon-counting-detector CT

Shaojie Chang, PhD[1], **Liqiang Ren, PhD**[1,†], **Shanshan Tang, PhD**[1,†], **Jeffrey F. Marsh Jr**[1], **Scott Hsieh, PhD**[1], **Cynthia H. McCollough, PhD**[1], **Shuai Leng, PhD**[1,*]

[1]Department of Radiology, Mayo Clinic, Rochester, MN, US

Abstract

Background: Coronary calcification is a strong indicator of coronary artery disease, and patients with a "zero" coronary calcification score have a much lower risk of future cardiac events than those with even small amounts of calcium. However, false-negative (incorrect zero scores) may occur if small calcifications are missed at CT due to limited spatial resolution.

Purpose: To demonstrate lower limits of detection for coronary calcification using an ultra-high-resolution (UHR) mode on a clinical photon-counting-detector CT (PCD-CT), compared to a conventional energy-integrating-detector CT (EID-CT).

Methods: Chicken eggshell fragments (0.4-0.8 mm) mimicking coronary calcifications were scanned on a clinical PCD-CT (NAEOTOM Alpha) in UHR mode and a conventional EID-CT (SOMATOM Force) with matched tube potential and radiation dose levels to the PCD-CT. PCD-CT images were reconstructed with a sharp kernel (Qr68) and a quantum iterative algorithm (QIR-3). Two sets of EID-CT images were reconstructed: routine clinical kernel (Qr36, ADMIRE-3) and a sharper kernel (Qr54) with similar noise to PCD-CT images. With institutional review board approval, *in vivo* exams performed with the PCD-CT in UHR mode were compared against patients' clinical EID-CT exams. The visibility of calcifications on PCD-CT and EID-CT images was assessed and compared qualitatively.

Results: PCD-CT images visualized all calcified fragments, while EID-CT failed to detect those below 0.6 mm using a routine protocol. EID-CT with Qr54 improved visibility but distorted boundaries. Calcifications were less visible on EID-CT than PCD-CT as phantom sizes increased. 0.6- and 0.7-mm calcified fragments were barely visible on 35- and 40-cm phantom EID-CT images. Patient cases showed small calcifications missed on EID-CT but detected on PCD-CT.

Conclusion: At matched radiation dose, PCD-CT in UHR mode provided higher spatial resolution and improved the detectability of small calcified fragments for different phantom/patient sizes in comparison to EID-CT.

[*]**Corresponding Author** Shuai Leng, PhD, 200 First Street SW, Rochester, MN 55905, USA, Phone: (507) 293-4233, Fax: (507) 266-3661, leng.shuai@mayo.edu.

[†]Current: Department of Radiology, UT Southwestern Medical Center, Dallas, TX, US

Conflict of Interest Statement

Cynthia McCollough is the receipt of a research grant to the institution from Siemens Healthineers. The other authors have no relevant conflicts of interest to disclose.

Keywords

Coronary artery disease; computed tomography (CT); photon-counting-detector CT; calcium score

1. Introduction

The presence of coronary calcification is a specific biomarker of coronary artery disease, and the extent of calcification measured using CT is an important predictor of future disease risk.[1-3] The Society of Cardiovascular Computed Tomography and the Society of Thoracic Radiology both recommend the evaluation of coronary calcification with CT, typically using electrocardiogram (ECG) gating, though even non-gated scans are increasingly recommended as acceptable.[4] Agatston score is a commonly used scoring method for coronary calcification in conventional CT scans with energy-integrating detectors (EIDs).[5] Images are usually reconstructed with 3 mm slices, and the final score is calculated as the sum of the scores for all individual calcified lesions (CT number value > 130 Hounsfield units (HU)) in all coronary arteries extending through the z-axis of the heart. Patients presenting with “zero” coronary calcification Agatston scores have a much lower risk of future cardiac events than those with even small amounts of calcium,[6-8] which is known as the "power of zero". Additionally, a study suggests that thin slice reconstructions (e.g., 0.5 mm) can more sensitively detect small amounts of coronary calcium, resulting in a positive calcium score for patients who had zero calcium scores in standard reconstruction.[9] Moreover, Urabe *et al.*[10] confirmed 0.5-mm thin-slice reconstruction for identifying small calcifications is useful for detecting coronary plaques and stenosis in patients with zero scores. However, smaller calcifications (e.g., < 0.5 mm) may not be detected due to the limited spatial resolution.

Photon-counting detector (PCD) CT is an emerging technology capable of directly converting incident X-ray photons into electrical signals, whereas EID uses an indirect conversion with visible light generated during an intermediate step.[11-13] With PCDs, physical septa are not required to prevent crosstalk of optical photons, allowing for smaller pixel sizes, as small as 0.2 mm at the isocenter of the CT gantry. However, the reduced size of detector elements comes with certain limitations, including charge sharing and the potential escape of fluorescence and scattered x-rays. These factors can negatively impact the spatial resolution and energy-resolving capability of PCDs, thereby compromising the overall performance of the system.[13] But the implementation of smaller detectors still enables ultra-high-resolution (UHR) CT imaging [1415] that is not possible with conventional EIDs. Despite the introduction of a CT system (Canon Precision) with the smallest EID elements (0.25 mm) for UHR imaging, its 10% modulation transfer function is still lower than 25 line pairs per centimeter, while the PCD CT system can achieve an increased 10% modulation transfer function of up to 36.1 line pairs per centimeter.[16] PCD-CT can thus produce a higher spatial resolution image, which reduces partial-volume effects and consequently may improve the detectability of small coronary calcifications.[17,18]

To explore the calcification detectability with PCD-CT, phantom studies were performed with calcium fragments ranging from 0.4 to 0.8 mm in 0.1 mm increments and scanned

within three anthropomorphic thoracic phantoms representing different patient sizes. This study aims to determine the detectability of sub-millimeter calcified fragments using a UHR PCD-CT system and to compare the calcium detection performance with a conventional state-of-the-art EID-CT scanner.

2. Methods

2.A. Phantom design

Calcification phantoms were built using boiled chicken eggshell (calcium carbonate) fragments, with thickness fixed at 0.4 mm. Detailed steps are shown in Figure 1(a). First, the eggshells were broken into fragments and measured using a vernier caliper. These fragments were then categorized into five size groups ranging from 0.4 to 0.8 mm, with increments of 0.1 mm. The choice of 0.4 mm as the minimum size was limited by the constraints of manual handling. Next, a solution was created using 5% gelatin by dry weight and 100 mL of distilled water. This solution was heated with continuous stirring until it clarified, which typically occurs when the temperature reaches the 90°C range. The clarified solution was poured into a plastic ice cube tray, filling each compartment halfway. The remaining solution was kept warm for later use. After cooling to room temperature (20°C) for approximately 15 minutes, the solution in the tray solidified. Calcified fragments were then placed on top of the solidified gel solution, with each fragment placed in a separate compartment. The fragments were randomly oriented in the solution to mimic realistic scenarios in patients. The remaining warm gel solution was added slowly and gradually to the tray to completely cover each calcification. It is important to note that adding the warm solution slowly prevents heat transfer to the solidified gel, which could cause it to become liquid again. Additionally, this stabilizes the positioning of each fragment so that it is suspended and fully surrounded by the gel solution. It was then left to cool completely before the CT scan. An example of a 0.4 mm specimen suspended in one compartment is shown in Figure 1(b). The ice cube tray was placed at the center of three anthropomorphic thoracic phantoms (QRM, lateral dimensions: 30, 35, and 40 cm) mimicking various patient sizes, as shown in Figure 1(c).

2.B. Data acquisition and image reconstruction

Each anthropomorphic phantom was scanned separately on a clinical PCD-CT (NAEOTOM Alpha, Siemens Healthineers) in a UHR mode (collimation: 120 x 0.2 mm, 0.2 mm pixel pitch is at the isocenter), and a conventional EID-CT (SOMATOM Force, Siemens Healthineers) with a 96 x 0.6 mm collimation. A tube potential of 120 kV was used for both systems. The clinical routine dose levels for phantoms of various sizes from the PCD-CT scan were used. Specifically, the phantoms were scanned on the PCD-CT using the clinical protocol, and the corresponding radiation doses (volume CT dose index: $CTDI_{vol}$) were recorded as 1.37, 2.07, and 3.27 mGy for the 30-, 35-, and 40-cm phantoms, respectively. Subsequently, the same phantoms were scanned on the EID-CT, with adjustments made to the x-ray tube current to achieve CTDIvol values of 1.37, 2.07, and 3.27 mGy, identical to those obtained from the PCD-CT, thereby ensuring a matched dose level. PCD-CT images were reconstructed with a quantum iterative reconstruction algorithm at strength 3 (QIR-3), 1024 x 1024 matrix, 200 mm field of view (FOV), 0.2 mm slice thickness, and a sharp

kernel (Qr68). EID-CT images were reconstructed following the routine clinical protocol at our institution with an iterative reconstruction algorithm at strength 3 (ADMIRE-3), 512 x 512 matrix, 200 mm FOV, 0.6 mm slice thickness, and a Qr36 kernel. An additional reconstruction of the EID-CT data was performed with a sharper Qr54 kernel that resulted in a similar noise level as that of the PCD-CT images. Details about the acquisition and reconstruction parameters are summarized in Table 1.

2.C. Detectability and image analysis

For each phantom size, the detectability of the calcium fragments from 0.4 mm to 0.8 mm on the EID-CT and PCD-CT images was visually assessed and compared. A circular region of interest (ROI) of approximately 0.25 cm^2 was placed in a uniform area of the gelatin to measure noise (standard deviation of CT numbers) on all image sets. The ROI position was initially identified in the PCD-CT image and then positioned identically on the EID-CT Qr36 and Qr54 images. To quantitatively assess the detectability, we employed a threshold of 130 HU, which is used in Agatston score to distinguish between background and calcium. Specifically, a 10×10 pixels patch surrounding the target calcification was identified and the voxel numbers that exceed the 130 HU within these regions were determined. The voxel numbers of calcium (Ca_VN) and false positives within the uniform region (FP_VN) were recorded and compared. Ideally, the count of false positives in the uniform region should be zero.

It is worth noting that PCD-CT systems weigh each individual photon equally, regardless of the measured photon energy. This characteristic leads to a more significant contribution of low-energy photons to the image contrast in PCD-CT compared to EID-CT (where photons are weighted based on their energies), resulting in an overall improvement in calcium CT number and image contrast. Therefore, a higher threshold should be applied in UHR PCD-CT, reconstructed in single-energy mode (T3D), to take this difference into consideration. To provide a comprehensive evaluation, we conducted scans on both PCD-CT and EID-CT using a torso-shaped phantom with a lateral width of 40 cm, which contained calcium at a concentration of 100 mg/cc. When comparing the mean CT numbers of the calcium ROI, we found that PCD-CT had a mean CT number of 344 HU, while EID-CT had a mean CT number of 305.2 HU. This resulted in a ratio of 1.13 for PCD-CT to EID-CT in the calcium area. Based on this ratio, we introduced an appropriate threshold of 150 HU for calcium detection on the PCD-CT scans, which was approximately calculated by multiplying the ratio of 1.13 with the 130 HU threshold used in EID-CT. Applying this threshold enables a meaningful assessment of PCD-CT's ability to detect calcifications. Moreover, in both experiments, a 4-connectivity constraint was utilized to effectively distinguish calcium from the background, a choice that is consistent with the one employed in the Agatston score calculation.

2.D. *In vivo* comparison

One sample patient retrospectively reviewed from an IRB-approved prospective study comparing coronary CTA exams between EID-CT and PCD-CT. The PCD-CT images were qualitatively compared against the EID-CT images that were reconstructed with the clinical

routine kernel and a sharp kernel, as done with the phantom studies. Calcification detection was visually assessed and compared between the EID-CT and PCD-CT exams.

3. Results

3.A. Detectability assessment

The detectability of calcified fragments was assessed from images acquired on 30-, 35-, and 40-cm phantoms with the PCD-CT and EID-CT and results are summarized in Figure 2. As shown in Figure 2(b), for PCD-CT, all calcified fragments (0.4 to 0.8 mm) were detected across all phantom sizes. For EID-CT with clinical routine Qr36 kernel, calcium fragments below 0.6 mm were not detectable for any phantom sizes. In the EID-CT images, detectability decreased substantially with increased phantom size, with the 0.6- and 0.7-mm calcified fragments hardly visible in the 35- and 40-cm phantoms.

As shown in Figure 2(b), the use the of a smooth kernel (Qr36) resulted in a substantial blurring of calcified fragments and much lower image noise on the EID-CT images. With the sharper kernel (Qr54), EID-CT images showed a similar noise level to PCD-CT. The noise values in the three image types are summarized in Table 2. We observed the following. First, the sharper kernel (e.g., Qr54 vs Qr36) improved the spatial resolution and calcium detection, albeit with increased image noise. As indicated by the white arrows in Figure 2(b), 0.5-mm calcifications can be detected on the Qr54 EID-CT images but not on the Qr36 images. Second, image noise increased with phantom size for both EID-CT and PCD-CT, as shown in the noise measurements in Table 2. Third, even at the same noise level, *i.e.,* PCD and EID-Qr54, EID-CT exhibited a blurrier appearance due to its lower image resolution. Additionally, more distortion of the calcified boundaries was found in EID-CT, as indicated by the white circle in Figure 2(b). PCD-CT maintained robust detectability for small calcifications in different phantom sizes, better than EID-CT.

In Figure 3, the quantitative results are consistent with the visual assessment, demonstrating that in PCD-CT, all calcified fragments ranging from 0.4mm to 0.8mm were detectable across all phantom sizes. However, it is important to note that there were some false positive voxels present in the uniform region, as indicated by non-zero FP_VN values. These false positives can be attributed to increased noise in high-resolution PCD-CT images. Nevertheless, when an appropriate threshold of 150 HU was applied to take into consideration of the photon weighting difference between EID-CT and PCD-CT, no FP_VN was observed, and the Ca_VN consistently matched the size of the calcifications.

On the other hand, in EID-CT, the results obtained with Qr36 did not yield quantitative detectability. Notably, the employment of the sharp kernel with Qr54 improved the detectability in comparison to the Qr36, resulting in an increase in the voxel number for calcifications ranging from 0.5mm to 0.8mm. However, it is important to note that the detected voxel count still did not align consistently with the size of the calcifications, as seen in PCD-CT using the 150 HU threshold. Moreover, the 0.4mm calcification in both EID-CT with both Qr36 and Qr54 kernels remained undetectable, which is consistent with the visual detection as depicted in Figure 2(b).

3.B. In vivo comparison

Sample images from the axial and coronal view of a patient scanned with the UHR PCD-CT and EID-CT are shown in Figure 4 as a clinical demonstration. In the PCD-CT images, both views showcase the remarkable spatial resolution, allowing for the detection of a small calcification (indicated by an arrow). Conversely, the small calcification remains undetectable in both views of the EID-CT images, utilizing both clinical routine and sharp kernels (Qr36 and Qr54).

4. Discussion

To explore the size limits of detectability using UHR PCD-CT, this study investigated the detectability of small-calcified fragments from 0.4 to 0.8 mm in comparison to EID-CT. These fragments, when placed within small-, medium- and large-phantoms, were reliably detected with PCD-CT. However, calcium fragments below 0.6 mm were not detectable on EID-CT with a routine clinical protocol for any phantom size. Even though the detectability was improved by using a sharper kernel (Qr36 to Qr54) in EID-CT compared to the routine images, the 0.4 mm calcium was still not detectable. Meanwhile, the *in-vivo* example demonstrated how UHR PCD-CT can outperform EID-CT in terms of small calcification detection.

A previous study evaluated calcification detection with an insert phantom containing 100 calcifications with diameters ranging from 0.5 to 2.0 mm using an investigational spectral PCD-CT scanner (SPCCT; Philips Healthcare) with 0.27 mm detector pixel pitch (at the isocenter).[18] The results showed superior calcification detectability for PCD-CT compared to an EID-CT (IQon Spectral CT, Philips Healthcare) from the same vendor. The study followed the Agatston methodology,[5] employing a slice thickness of 3.0 mm. In a separate investigation[19], it was confirmed that employing a reconstruction with a thin slice thickness of 0.67 mm from a prototype SPCCT could enhance the calcium detectability. In contrast, our study focuses on investigating the detectability of small calcifications by utilizing the UHR mode of the first clinical PCD-CT, which incorporates an ultra-thin slice thickness of 0.2 mm. Calcium fragments as small as 0.4 mm were included in our study, and 3 phantom sizes were included to investigate the influence of patient size on detectability of small calcifications. As shown in our results, the high spatial resolution of PCD enabled calcification detection in phantoms, which was corroborated with sample patient images.

Our study has several limitations. First, this study employed noise standard derivation to assess matched noise levels between PCD-CT and EID-CT images for comparison purposes. Nonetheless, it is important to acknowledge that although the reconstructed images have identical noise standard derivations, the noise-power-spectrum may differ between the two systems, resulting in different behaviors for the given task. Hence, more comprehensive studies are warranted for an evaluation of the task of detecting small calcifications with PCD-CT and EID-CT. This could either be conducted using model observers which take into consideration of imaging task (e.g., calcium object) and imaging system characteristics (e.g., MTF and NPS), or formal reader studies of diagnostic performance (e.g., sensitivity and specificity) from in vivo non-contrast coronary calcium exams. Second, this study only focused on the detectability of small calcium fragments. The smooth Qr36 kernel is

the recommended choice for the current clinical task of coronary calcium detection and quantification because it provides precise CT numbers and maintains a reasonable balance between dose and image quality (e.g., noise). In the future, it would be interesting to compare the performance of PCD-CT using the clinical protocol for calcium Agatston scoring with EID-CT. Additionally, our future research will incorporate a comprehensive investigation of false positive analysis within the entire volume of both PCD-CT and EID-CT images. This aspect is essential to provide a more holistic understanding of the system's performance and its potential effect on calcium scoring. Although the smooth Qr36 kernel may not resolve smaller calcifications, several studies have emphasized the importance of detecting such small calcifications for coronary CTA.[9,10] How the increased detectability of very small calcification would affect coronary artery calcium (CAC) scoring requires further investigation.[5,20-22] Fourth, another important feature enabled by UHR PCD-CT is the simultaneous acquisition of multi-energy data, allowing for the generation of virtual monoenergetic images (VMIs). It is worth considering the potential impact of utilizing lower energy VMIs to enhance contrast and higher energy VMIs to mitigate calcium blooming artifacts[23] on the detectability of small calcifications. Furthermore, future studies will incorporate additional in-vivo investigations, with a particular focus on the analysis of false positive cases related to PCD-CT and exploring their clinical impact.

5. Conclusion

At matched radiation dose, PCD-CT provided higher spatial resolution images and more robust detectability of small calcifications compared to EID-CT. This means that PCD-CT was able to capture and identify calcified fragments ranging from 0.4mm to 0.8mm in size, which might have been missed by EID-CT. This detection capability was consistent across all phantom sizes, as visually observed and quantitatively measured. The improved detectability of calcifications with PCD-CT may allow a more accurate assessment of risk of cardiovascular events in patients with very small calcifications. However, the clinical relevance of the very small calcifications needs to be investigated in future studies.

Acknowledgments

Research reported in this article was supported by the National Institutes of Health under award number R01EB028590. The content is solely the responsibility of the authors and does not necessarily represent the official views of the National Institute of Health. Authors would like to thank Kevin Kimlinger for his assistance with manuscript preparation and submission.

References

1. Detrano R, Guerci AD, Carr JJ, et al. Coronary calcium as a predictor of coronary events in four racial or ethnic groups. New England Journal of Medicine. 2008;358(13):1336–1345. [PubMed: 18367736]
2. Greenland P, Alpert JS, Beller GA, et al. 2010 ACCF/AHA guideline for assessment of cardiovascular risk in asymptomatic adults: a report of the American College of Cardiology Foundation/American Heart Association task force on practice guidelines developed in collaboration with the American Society of Echocardiography, American Society of Nuclear Cardiology, Society of Atherosclerosis Imaging and Prevention, Society for Cardiovascular Angiography and Interventions, Society of Cardiovascular Computed Tomography, and Society for Cardiovascular Magnetic Resonance. Journal of the American College of Cardiology. 2010;56(25):e50–e103. [PubMed: 21144964]

3. Polonsky TS, McClelland RL, Jorgensen NW, et al. Coronary artery calcium score and risk classification for coronary heart disease prediction. Jama. 2010;303(16):1610–1616. [PubMed: 20424251]
4. Hecht HS, Cronin P, Blaha MJ, et al. 2016 SCCT/STR guidelines for coronary artery calcium scoring of noncontrast noncardiac chest CT scans: a report of the Society of Cardiovascular Computed Tomography and Society of Thoracic Radiology. Journal of cardiovascular computed tomography. 2017;11(1):74–84. [PubMed: 27916431]
5. Agatston AS, Janowitz WR, Hildner FJ, Zusmer NR, Viamonte M Jr, Detrano R. Quantification of coronary artery calcium using ultrafast computed tomography. Journal of the American college of cardiology. 1990;15(4):827–832. [PubMed: 2407762]
6. Blaha MJ, Mortensen MB, Kianoush S, Tota-Maharaj R, Cainzos-Achirica M. Coronary artery calcium scoring: is it time for a change in methodology? JACC: Cardiovascular Imaging. 2017;10(8):923–937. [PubMed: 28797416]
7. Hecht H, Blaha MJ, Berman DS, et al. Clinical indications for coronary artery calcium scoring in asymptomatic patients: expert consensus statement from the Society of Cardiovascular Computed Tomography. Journal of cardiovascular computed tomography. 2017;11(2):157–168. [PubMed: 28283309]
8. Blaha MJ, Cainzos-Achirica M, Greenland P, et al. Role of coronary artery calcium score of zero and other negative risk markers for cardiovascular disease: the Multi-Ethnic Study of Atherosclerosis (MESA). Circulation. 2016;133(9):849–858. [PubMed: 26801055]
9. van der Bijl N, de Bruin PW, Geleijns J, et al. Assessment of coronary artery calcium by using volumetric 320-row multi-detector computed tomography: comparison of 0.5 mm with 3.0 mm slice reconstructions. The international journal of cardiovascular imaging. 2010;26:473–482. [PubMed: 20072817]
10. Urabe Y, Yamamoto H, Kitagawa T, et al. Identifying small coronary calcification in non-contrast 0.5-mm slice reconstruction to diagnose coronary artery disease in patients with a conventional zero coronary artery calcium score. Journal of Atherosclerosis and Thrombosis. 2016;23(12):1324–1333. [PubMed: 27397477]
11. Rajendran K, Petersilka M, Henning A, et al. First clinical photon-counting-detector CT system: Technical evaluation. Radiology. 2022;303(1):130. [PubMed: 34904876]
12. Flohr T, Ulzheimer S, Petersilka M, Schmidt B. Basic principles and clinical potential of photon-counting detector CT. Chinese Journal of Academic Radiology. 2020;3:19–34.
13. Leng S, Bruesewitz M, Tao S, et al. Photon-counting detector CT: system design and clinical applications of an emerging technology. Radiographics. 2019;39(3):729–743. [PubMed: 31059394]
14. Leng S, Rajendran K, Gong H, et al. 150-μm spatial resolution using photon-counting detector computed tomography technology: technical performance and first patient images. Investigative radiology. 2018;53(11):655–662. [PubMed: 29847412]
15. Leng S, Yu Z, Halaweish A, et al. Dose-efficient ultrahigh-resolution scan mode using a photon counting detector computed tomography system. Journal of Medical Imaging. 2016;3(4):043504-043504.
16. Willemink MJ, Grist TM. Counting Photons: The Next Era for CT Imaging? In. Vol 303: Radiological Society of North America; 2022:139–140.
17. Boccalini S, Si-Mohamed SA, Lacombe H, et al. First in-human results of computed tomography angiography for coronary stent assessment with a spectral photon counting computed tomography. Investigative Radiology. 2022;57(4):212. [PubMed: 34711766]
18. van der Werf N, Rodesch P, Si-Mohamed S, et al. Improved coronary calcium detection and quantification with low-dose full field-of-view photon-counting CT: a phantom study. European Radiology. 2022:1–11.
19. van der Werf NR, Si-Mohamed S, Rodesch P, et al. Coronary calcium scoring potential of large field-of-view spectral photon-counting CT: a phantom study. European radiology. 2022;32:152–162. [PubMed: 34255159]

20. McCollough CH, Ulzheimer S, Halliburton SS, Shanneik K, White RD, Kalender WA. Coronary artery calcium: a multi-institutional, multimanufacturer international standard for quantification at cardiac CT. Radiology. 2007;243(2):527–538. [PubMed: 17456875]

21. Greenland P, LaBree L, Azen SP, Doherty TM, Detrano RC. Coronary artery calcium score combined with Framingham score for risk prediction in asymptomatic individuals. Jama. 2004;291(2):210–215. [PubMed: 14722147]

22. Shea S, Navas-Acien A, Shimbo D, et al. Spatially weighted coronary artery calcium score and coronary heart disease events in the multi-ethnic study of atherosclerosis. Circulation: Cardiovascular Imaging. 2021;14(1):e011981. [PubMed: 33461306]

23. Chang S, Huber NR, Marsh JF, et al. Pie-Net: Prior-information-enabled deep learning noise reduction for coronary CT angiography acquired with a photon counting detector CT. Medical physics. 2023.

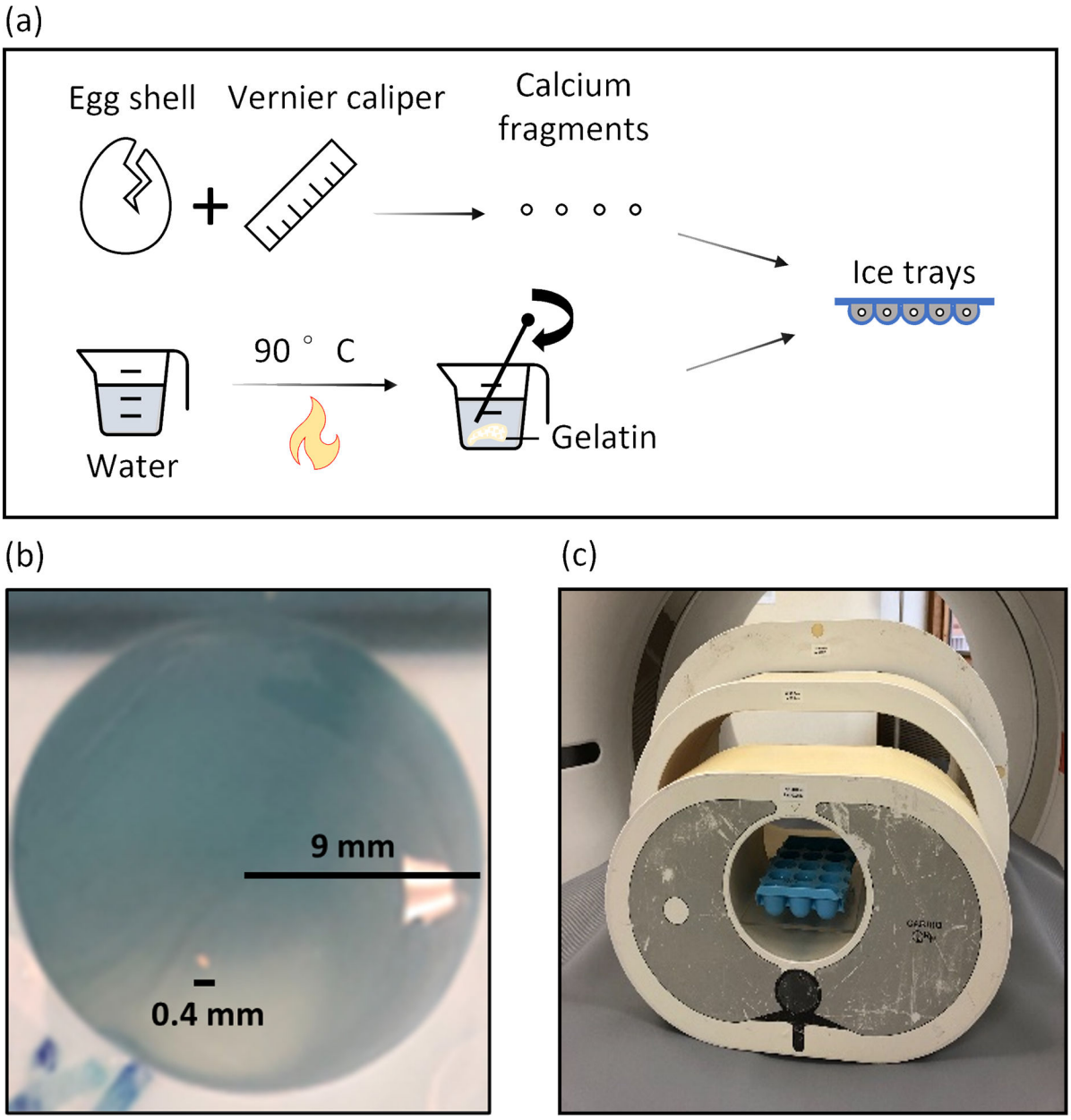

Figure 1.

Illustration of the experimental setup. (a) The process of calcium fragment preparation. (b) Photo of a 0.4 mm calcium fragment embedded in the gelatin in one tray (9-mm compartment diameter). (c) Ice cube trays with eggshell fragments were placed in one of three anthropomorphic phantoms (QRM, lateral width of 30, 35, and 40 cm).

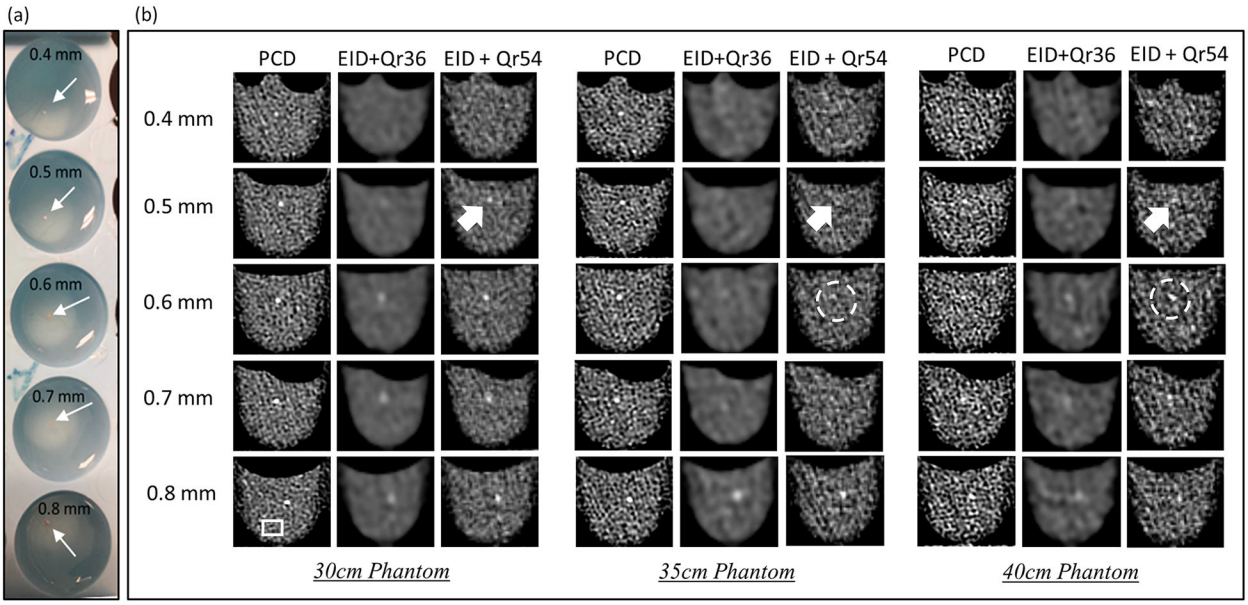

Figure 2.

(a) Photos of the scanned phantom. (b) Sample images from PCD-CT and EID-CT with a routine clinical kernel Qr36 and a sharp kernel Qr54 (similar noise level as PCD-CT). All calcium fragments (0.4 to 0.8 mm) were detectable in PCD-CT images across all phantom sizes. Compared to both the routine and sharp kernel EID-CT images, the PCD-CT images yielded improved visualization of calcification details, better delineation of object boundaries, and better calcium detection. Display window level (WL) / window width (WW): 40/400.

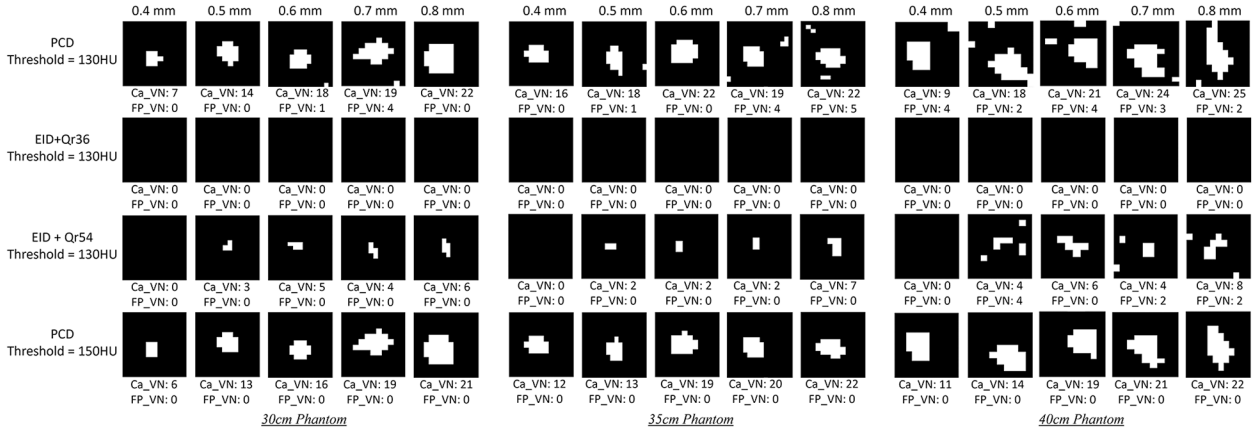

Figure 3.

Quantitative detectability assessment results. The ROIs were selected to encompass the detected calcifications and adjacent uniform regions near calcium, using a 10×10 patch. The voxel numbers associated with these regions, exceeding the predetermined threshold, were recorded as Ca_VN and FP_VN, respectively.

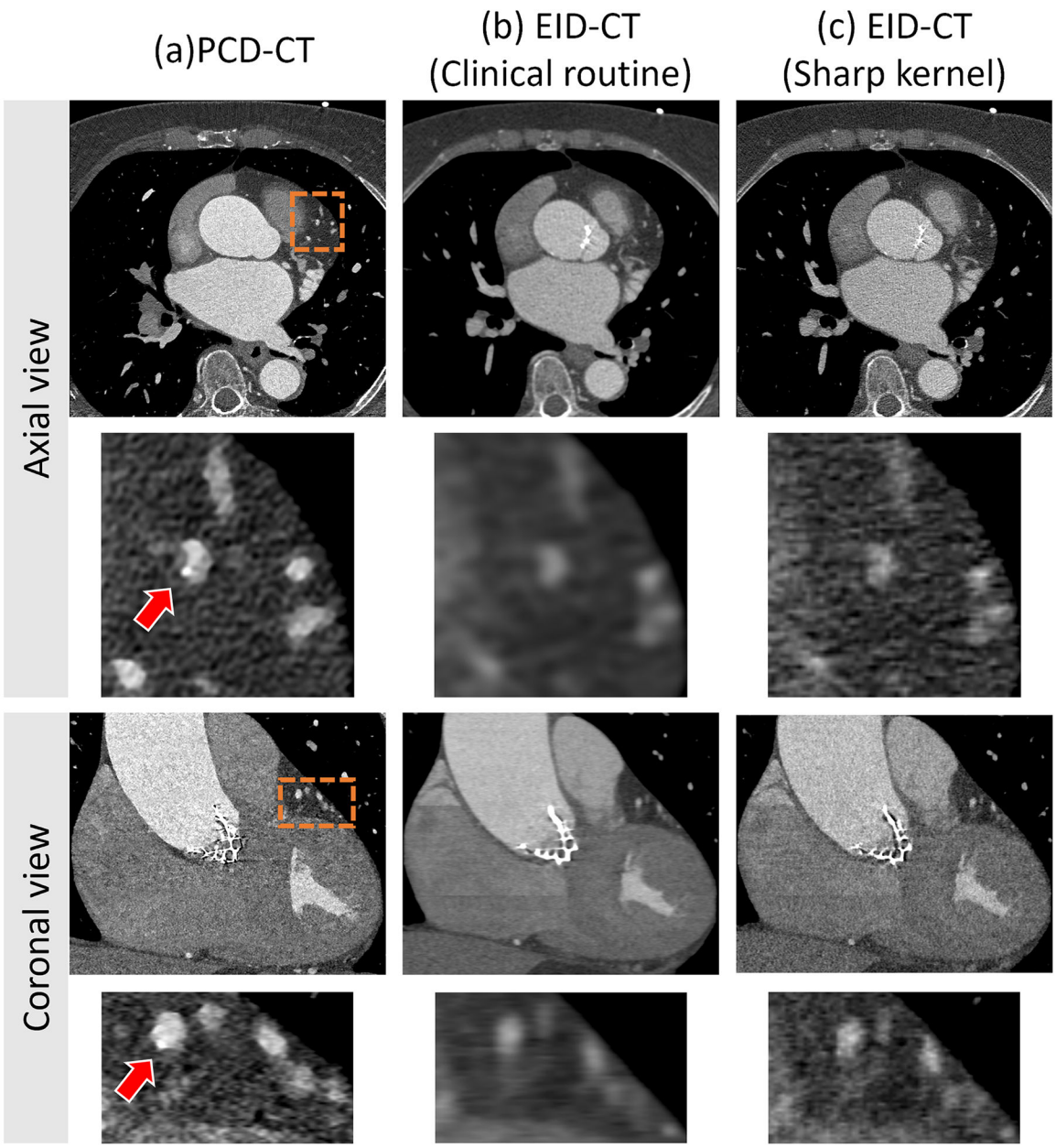

Figure 4.

Sample images of small calcium detection in patients. Axial and coronal view of PCD UHR (a), EID-clinical routine (b), and EID-sharp kernel (c) CT images of a coronary CTA in a 77-year-old man show that high spatial resolution enabled detection of the very small calcification (arrow in (a)). Image display window (WL/WW: 200/1000 HU).

Table 1.

Scan and reconstruction parameters used in the PCD-CT and EID-CT

Parameter	EID-CT	PCD-CT
Scanner model	SOMATOM Force	NAEOTOM Alpha
kV	120	
Effective mAs	20 (30cm)	17 (30cm)
	31 (35cm)	26 (35cm)
	49 (40cm)	41 (40cm)
CTDIvol (mGy)	1.37 (30cm), 2.07 (35cm), 3.27 (40cm)	
Collimation (mm)	192 × 0.6	120 × 0.2
Pitch	0.6	
Rotation Time (s)	0.25	
Reconstruction	ADMIRE-3	QIR-3
Kernel	Qr36, Qr54	Qr68
Slice thickness (mm)	0.6	0.2
Increment (mm)	0.3	0.1
Reconstruction field of view (mm)	200	
Image matrix size	512 × 512	1024 × 1024

Table 2.

Noise measurement in EID- and PCD-CT images of different phantom sizes (Unit: HU)

Phantom size	PCD-CT(Qr68)	EID-CT (Qr36)	EID-CT (Qr54)
30cm	42.9	9.7	42.7
35cm	55.7	11.5	57.1
40cm	67.9	16.1	67.2